Biodistribution and Dosimetry of Iodine-123-IBF: A Potent Radioligand for Imaging the D2 Dopamine Receptor

P. David Mozley, James B. Stubbs, Hank F. Kung, Mark H. Selikson, Michael G. Stabin and Abass Alavi

Division of Nuclear Medicine and Department of Radiology, University of Pennsylvania, Philadelphia, Pennsylvania; and the Radiation Internal Dose Information Center, Oak Ridge Institute for Science and Education, Oak Ridge, Tennessee

Iodine-123-labeled iodo-benzofuran (IBF) is a potent D2 dopamine receptor antagonist that has been developed as a potential SPECT imaging agent. This report documents its biodistribution and radiation dosimetry in seven healthy humans. Approximately 100 MBq of IBF were administered to each volunteer. Urine was collected to measure the fraction of the activity that was voided by the renal system. Conjugate images were serially acquired over 24 hr to determine the fraction of activity in the other organs. Standard image analysis techniques were used to measure the geometric mean count rates in the brain, GI tract, heart, liver, lungs and thyroid at each time point. Corrections for attenuation were made with ^{123}I transmission scans. Multicompartmental modeling was used to simulate and predict the biokinetic behavior of ^{123}I-IBF in the rest of the body. The absorbed doses for 24 organs were then estimated with the MIRD formalism. Rapid biological washout minimized the absorbed dose to most tissues. The excretory organs were exposed to the most radiation. The lower large intestine received about 0.13 mGy/MBq (0.48 rad/mCi), and the urinary bladder received 0.11 mGy/MBq. This low radiation burden will allow more than 370 MBq (10 mCi) to be administered to healthy research subjects during each study of the D2 receptor. Since high quality images of the brain can be obtained with half this amount, the findings suggest that ^{123}I-labeled IBF has a large margin of radiation safety in humans. Its stability in vivo and its high target-to-background contrast ratio in the human brain may make it a useful SPECT imaging agent.

J Nucl Med 1993; 34:1910–1917

Dopamine plays an important role in the mediation of cognition, emotion and movement (*1*). Neuroimaging studies of the dopaminergic system may further our understanding of normal cerebral function and the pathophysiology of several brain disorders (*2*). The D2 dopamine receptor subtype has been the subject of particularly intense investigation because it may be intimately involved in the initiation and maintenance of several neuropsychiatric symptoms (*3–5*). It appears to be an important site of action for a number of therapeutic medicines (*6–8*) and several drugs of abuse (*9–12*).

Many substituted benzamide derivatives are potent D2 dopamine receptor antagonists (*13*). Iodination can sometimes substantially increase both their affinity and specificity for the D2 receptor (*14*). Since the single photon emitted by iodine-123 (^{123}I) has highly favorable physical imaging characteristics, a number of iodinated benzamides have been developed that can be used with single photon emission computed tomography (SPECT) to study the D2 receptor in humans (*15–19*). Most of the initial clinical trials with these ligands have shown that they localize in the dopaminergic regions of the diencephalon and mesotemporal lobes (*20–29*). However, the search for new ligands has continued because the target-to-background contrast ratio that can be obtained with some of these agents in clinical practice has been limited to <2:1 (*20*).

In order to increase the target-to-background contrast ratio in the D2 dopaminergic regions of the brain, we developed an iodinated benzamide with a fused ring structure called IBF (*30,31*). The D2 receptor is selectively bound by 5-iodo-7-N-[(1-ethyl-2-pyrrolidinyl)-methyl] carboxamido-2,3-dihydrobenzofuran (IBF) with a Kd of 0.106 ± 0.001 n*M* and a B max of 246 ± 20 fmol/mg protein in striatal membrane preparations excised from rats (*30*). At 2 hr after intravenous injection, the localization of IBF in the striatum is 48 times greater than the nonspecific activity in cerebellum of rats (*30*). Investigations in living rodents and nonhuman primates have demonstrated that it is possible to displace IBF from its specific binding sites in the basal ganglia with both directly and indirectly acting dopaminergic drugs (*30,31*). A preclinical study of its pharmacological safety suggested that nonradioactive IBF does not produce any observable toxic effects in rabbits, even when administered in doses that are several orders of magnitude higher than the amounts that are needed for radiotracer studies (unpublished data). These findings led to this study of its biodistribution and radiation dosimetry in humans.

Received Dec. 30, 1992; revision accepted Jun. 20, 1993.
For correspondence or reprints contact: P. David Mozley, MD, 110 Donner Building, H.U.P., 3400 Spruce St., Philadelphia, PA 19104.

METHODS

Radionuclide

The Na ^{123}I used in this study was obtained commercially (Nordion Intl., Kanata, Canada). It was produced with an enriched xenon-124 target. The manufacturer guaranteed that the radionuclidic purity of each dose exceeded 99.8% at the time of our calibration. Impurities could have potentially included trace amounts of tellurium-121 (<0.05%), ^{124}I (<10^{-4}%), ^{125}I (<0.02%) and ^{126}I (<10^{-4}%) (Abeysekera B., Nordion Intl., *personal communication*, 1993). The specific activity of the ^{123}I was 2.4×10^5 Ci/mmol.

Radiolabeling

The preparation of the tributyl tin precursor has already been described in detail (*30*). The radiolabeling process began by adding about 12 mCi of Na ^{123}I to a kit containing 50 μg of 5-tri-butylstannyl-7-N(1-ethyl-2-pyrolidinyl-methyl)-carboxamido-2,3-dihydrobenzofuran. The iodination reaction was initiated with 50 μl of a 3% hydrogen peroxide solution and quenched 20 min later with 30 mg of sodium bisulfite. Sodium bicarbonate was added to bring the pH to about 7. The solution was then extracted with ethyl acetate three times. The combined extracts were passed through a column containing anhydrous sodium sulfate. The anhydrous ethyl acetate eluent was condensed to dryness under a stream of nitrogen gas. The residue was redissolved in 50 μl of ethanol and injected into a high-pressure liquid chromatography (HPLC) system consisting of a PRP-1 reverse-phase column eluted with acetonitrile-pH 7.0 buffer ammonium phosphate (5 m*M*, 90:10). The fraction of the eluent corresponding to ^{123}I-IBF was separated and collected. Ascorbic acid (100 μg) was added before the solution was condensed. The residue was then redissolved in 100 μl of ethanol and diluted with 3 ml of saline. The final solution was passed through a 0.22-μm filter prior to administration. A small volume of the final solution was removed and analyzed for purity with HPLC. Other aliquots were retained for sterility and pyrogenicity tests.

The theoretical specific activity of the no-carrier added ^{123}I-IBF was 240,000 Ci/mmol (*30*). However, the detection limits of the UV spectrometer that was used during this clinical study limited the measurements of specific activity to simply >50,000 Ci/mmol. The total labeling yield was 80%, and the radiochemical purity of the final product was >95%.

Subject Accrual and Assessment

The protocol was approved by the Internal Review Board and the Radioactive Drug Research Committee. Seven men with a mean age of 31.0 ± 7.9 yr (range: 20–41 yr) gave informed consent for the study. A structured medical history and physical examination indicated that they were healthy. None of them had a history of a disease process that could have affected the biodistribution or elimination of the radioligand.

Each subject presented at about 15:30 hr (3:30 p.m.). Blood was drawn for routine laboratory analyses as soon as they arrived and 24 hr after the administration of the tracer. The clinical laboratory battery included a complete blood cell count with differential, serum electrolytes, liver enzymes, thyroid function tests, an autoimmune panel, a urinalysis and a urine drug screen. Each subject was administered ten drops of Lugol's solution immediately after their blood was drawn for the initial laboratory studies. The tracer was administered about 1 hr later.

Linear Attenuation Measurements

A transmission source was prepared by dissolving 150–300 MBq of ^{123}I in about 500 ml of water in a sheet flood made of lucite. Nonattenuated images of the transmission sources positioned 35 cm from the surface of the collimator contained an average of 578 kct/2 min (range 406–1,100 kcts/2 min). Each subject was positioned between this sheet source and the gamma camera so that the mid-coronal plane of the body was 35 cm away from the surface of a parallel-hole collimator. Transmission images of the head, chest, abdomen and pelvis were then acquired for 2 min each. The counts that were transmitted through each organ were compared to the counts in the corresponding image of the flood taken without the subjects in the field of view.

Administered Activity Measurements

The amount of radioactivity in each syringe containing ^{123}I-IBF was measured in a dose calibrator before and after injection. The mean dose administered in this study was 94 MBq (2.5 mCi), with a range of 61–185 MBq (1.64–5.0 mCi). Quantitative images of the syringes were also acquired on the computer before and after administration. The acquisition parameters for the images of the syringes were identical to the ones that were used to scan the patients and acquire the transmission images. Images of the injection sites were checked to make sure that the doses had not infiltrated the subcutaneous tissue.

Emission Images

Conjugate images were obtained for 2 min each on a single-headed SPECT system (GE Medical Systems, Milwaukee, WI). The camera was equipped with a large field of view, low-energy, all-purpose, parallel-hole collimator. A 20% window was symmetrically centered on 159 keV. The first set of images was acquired about 1 hr after the administration of the ligand. Altogether, between four and six sets of emission images were obtained over the next 9 hr. Another set of images was acquired the next day.

Count Rate Measurements

Regions of interest (ROIs) were drawn with a digital track ball along the outer border of those organs that extracted enough activity to be seen clearly on the images (see Tables 2 and 4). An automated subroutine measured the number of pixels and the total counts in these ROIs.

The edges of many organs became progressively more obscure over time as the tracer was eliminated. When the boundaries of an organ could no longer be clearly visualized, the total number of counts in each view was estimated from the mean counts per pixel in the center of the organ. The process began by placing a limited ROI in the center of the organ. The ROI was made as large as possible while still ensuring that it fell completely within the organ. The average counts per pixel in each centrally limited ROI was then multiplied by the total number of pixels in the whole organ. The total number of pixels in the whole organ was measured on the earliest image of it by drawing a boundary right on its edges.

Organ Residence Times

The count rates in each ROI were corrected for decay and attenuation. Time-activity curves were generated from the geometric mean active in the brain, heart, liver, lungs and thyroid. The time-activity curves for these organs and the other tissues in the body were fitted with a multicompartmental model that was developed specifically to estimate organ residence times from the experimental data. The Simulation Analysis and Modeling (SAAM) (*32,33*) software used to mathematically fit the experi-

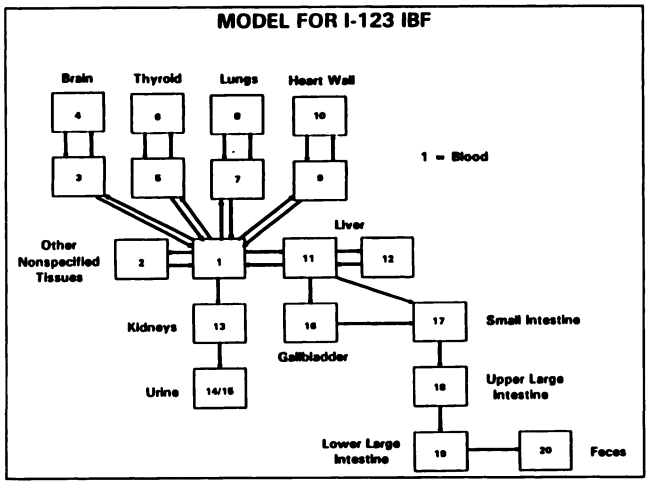

FIGURE 1. Multicompartmental model used to describe the biokinetics of the ^{123}I-labeled IBF. Numerical values for the intercompartmental transfer rates are listed in Table 1 for each of the seven subjects.

mental data to the multicompartmental model did not make any assumptions about the mechanism of IBF metabolism or its pharmacokinetic behavior other than its tissue distribution and excretion pathways. The model is schematically illustrated in Figure 1.

Cumulative urine activity measurements were used to model urinary excretion rates and predict fecal excretion fractions. Cumulative urinary excretion measurements were fitted to the compartmental model with SAAM software (*32*). Figure 1 illustrates the pathway from the central compartment to the kidneys, L(13,1), and from the kidneys to the urinary bladder, L(14,13). The cumulated bladder activity was calculated by assuming that the bladder voiding interval was only once per 4.8 hr, or five times a day (*34*).

Activity not excreted in the urine was assumed to be eliminated in the feces. The images suggested that most, if not all, of the bowel activity entered the gastrointestinal (GI) tract with the flow of bile after being cleared by the liver. Activity was never visible in the stomach. It was assumed that 30% of the activity excreted in the bile filled the gallbladder; the other 70% was assumed to flow directly into the small intestine (*35*). The early images of the right upper quadrant tended to corroborate this. The model assumed that the gallbladder ejected its contents into the duodenum in response to a meal once every 6 hr (*36*). The gallbladder contraction phase was assumed to last for 2 hr. Filling occurred during the other 4 hr of the cycle. The transfer rate coefficient of 1.8 hr^{-1} from the gallbladder to the small intestine was derived by taking the grand mean of the average emptying rates reported in three other studies (*35–37*). The gallbladder residence times were calculated by integrating the activity retention times predicted by the multicompartmental model. The activity entering the duodenum with the flow of bile was assumed to be transferred through the alimentary canal according to the kinetic model for the GI tract in ICRP 30 (*38*). The standard mass of tissue in each region of the gut was taken from ICRP 23 (*39*).

Estimates of the transfer rate coefficients L_i from the central compartment to the excretory compartments were made by calculating the uptake half-times in the kidney and liver. The other transfer rate coefficients were calculated with the SAAM software by allowing the program to adjust the value of each transfer coefficient L_i in the model in order to find a better fit of the data and model in the statistical sense. The process was launched with initial values for the transfer coefficients that were somewhat arbitrary, because they were based on prior experience with similar models for other tracers. The SAAM software then iteratively adjusted the values of the transfer coefficients L_i until a local minima was found in an N dimensional solution space, where N was the number of unknown variables in the model. The residence times were calculated by integrating the eigenvalues and eigenvectors which satisfied the coupled differential equations describing the model over time. These residence times were then used to estimate the absorbed doses for each individual subject with the MIRD technique (*40*) for the adult male phantom (*41*).

Most organs were modeled as the sum of two compartments. The kidneys, urinary bladder, gallbladder, small bowel and colon were all treated as single compartments. The remainder of the body residence times were estimated by the integration of the activity predicted to be retained in compartments 1 and 2 of the model.

RESULTS

HPLC demonstrated that the radiochemical purity of the ^{123}I-IBF used in the study of the human volunteers exceeded 95%. Pyrogenicity and sterility tests were all negative.

Images of the injection sites showed that the dose was partially infiltrated in only one subject. In this one case, quantification demonstrated that less than 1% of the activity in the injection syringe was left in the antecubital fossa after 1 hr. The measured count rates in the images of the other syringes ranged from 210 to 440 kcounts per min. There was no evidence to suggest that these count rates ever approached the saturation rate of the camera.

There were no subjective effects of the radiotracer on any of the subjects. Their vital signs remained stable throughout the procedure, and there were no changes noted on physical examination. There were no meaningful changes in any of the clinical laboratory assays performed on the blood specimens obtained 24 hr after tracer administration.

Table 1 lists the compartmental model parameters that were applied to the data. The data set from each subject was fitted independently. The values that were derived for the transfer rate coefficients were used to calculate the organ residence times. Table 2 lists the residence times in hours for all seven subjects. The values were highest in the bladder of five subjects, and highest in the colon for the other two. Table 3 shows their urine and fecal excretion fractions. Most of the dose was eliminated by the renal system in five of seven the volunteers.

Figure 2 shows the time-activity curves for the first subject. The agreement between the measured values and the values predicted by the model never differed by more than 10% in any of the subjects.

Figure 3 shows the cumulative urine activity curves for the subjects with the highest and the lowest fecal excretion fractions. There was good agreement between their experimental data and the fitted values. In the other cases, the

TABLE 1
Iodine-123-IBF Compartmental Model Parameter Values for Seven Normal Volunteers

	Rate Coefficient (hr^{-1})						
	Volunteer no.						
Parameter*	1	2	3	4	5	6	7
L(13,1)	3.54	1.70	7.20	5.92	8.73	5.51	5.30
L(14,13)	0.74	0.33	0.95	0.63	0.49	0.66	0.45
L(1,2)	3.90	1.17	2.92	3.90	4.12	0.0	0.070
L(2,1)	0.0	1.46	0.0	0.0	10.0	0.0	0.47
L(1,3)	0.43	0.74	0.82	0.50	0.80	0.90	0.90
L(3,1)	0.70	0.67	2.0	1.03	1.4	0.67	1.50
L(4,3)	0.011	0.015	0.006	0.006	5.9E-3	0.011	0.011
L(3,4)	0.0	0.006	0.001	0.004	4.0E-3	0.0	0.0
L(1,5)	1.20	0.35	0.70	0.30	0.58	0.68	0.65
L(5,1)	0.046	0.010	0.098	0.026	0.075	0.055	0.065
L(6,5)	0.050	0.010	0.047	0.010	0.004	8.0E-3	0.047
L(5,6)	0.065	0.0	0.145	0.0	0.0	0.0	0.11
L(1,7)	0.60	0.32	0.90	0.75	0.75	0.71	1.65
L(7,1)	4.95	1.20	7.0	8.5	5.5	2.40	6.60
L(8,7)	0.024	0.11	0.50	5.4E-3	3.4E-3	7.5E-3	0.22
L(7,8)	0.0	6.9E-4	0.46	0.0	0.0	6.9E-4	0.195
L(1,9)	1.30	0.28	0.80	0.80	0.80	0.81	0.80
L(9,1)	1.01	0.25	1.14	1.90	1.0	0.78	0.62
L(10,9)	0.015	0.12	0.125	0.010	5.5E-3	0.012	0.13
L(9,10)	0.035	0.012	0.31	0.035	0.035	0.012	0.17
L(11,1)	8.80	3.90	9.0	10.0	10.0	5.62	4.50
L(1,11)	5.9E-4	0.0	0.27	0.425	0.67	0.58	0.35
L(12,11)	0.042	0.48	0.016	0.011	0.025	0.038	0.050
L(11,12)	9.0E-3	0.25	0.016	0.0	0.105	0.040	0.11
L(17,11)	0.47	0.82	0.11	0.12	0.085	0.050	0.18
L(16,11) = 0.4286*L(17,11)							
L(17,16)	1.80	1.80	1.80	1.80	1.80	1.80	1.80
L(18,17)	0.25	0.25	0.25	0.25	0.25	0.25	0.25
L(19,18)	0.077	0.077	0.077	0.077	0.077	0.077	0.077
L(20,19)	0.042	0.042	0.042	0.042	0.042	0.042	0.042

*The parameter, L(n,p), is read as the rate at which material in compartment n arrives from compartment p.

differences between the experimental data and the values derived from the model were never more than 10%.

IBF was excreted primarily by the renal system in five of the seven subjects, who voided over half the administered activity within 8 hr of the administration. The mean predicted fecal excretion fraction for these five subjects was

TABLE 2
Residence Times (hr) in Each Organ

	Subject						
Organ	1	2	3	4	5	6	7
Bladder	0.76	0.63	1.60	1.38	1.74	2.02	1.49
Brain	0.13	0.17	0.21	0.19	0.16	0.13	0.23
Gallbladder	0.50	0.50	0.17	0.18	0.09	0.08	0.16
Heart wall	0.067	0.14	0.14	0.24	0.11	0.16	0.14
Kidney	0.34	0.74	0.59	0.84	1.39	0.72	1.28
Liver	1.49	1.29	1.83	1.77	1.17	1.51	1.05
Lungs	0.82	0.63	1.12	1.18	0.63	0.54	0.86
Small bowel	1.88	1.83	0.75	0.80	0.39	0.32	0.66
ULI	3.63	3.54	1.44	1.54	0.76	0.62	1.27
LLI	2.97	2.90	1.18	1.26	0.62	0.51	1.04
Thyroid	0.004	0.005	0.013	0.008	0.011	0.013	0.014
Remainder	0.076	0.36	0.082	0.10	0.29	0.28	0.58

SI = small intestine; ULI = upper large intestine; and LLI = lower large intestine.

TABLE 3
Urine and Fecal Extraction Fractions

Organ	Subject 1	2	3	4	5	6	7
Measured f_u	0.28	0.28	0.65	0.60	0.77	0.89	0.60
Predicted f_u	0.27	0.30	0.66	0.63	0.82	0.85	0.61
Predicted f_f	0.69	0.69	0.31	0.31	0.15	0.10	0.26

f_u = fraction of the administered activity excreted in the urine and f_f = fraction of the administered activity excreted in the feces.

0.23 (range 0.11–0.40). The other two subjects only voided 28% of the activity in their urine. The mean urinary clearance for all subjects was 58% ± 21%.

The organs of excretion received the largest doses of radiation. The target organ is the distal colon. It absorbs 0.13 ± 0.085 mGy/MBq (0.48 rad/mCi). The radiation burden to the proximal colon is almost as high as 0.12 ± 0.079 mGy/MBq, followed by the doses to the urinary bladder wall (0.11 ± 0.034 mGy/MBq), the kidneys (0.083 mGy/MBq ± 0.032 mGy/MBq) and the gallbladder (0.073 ± 0.047 mGy/MBq).

Table 4 lists the absorbed dose estimates for ^{123}I-IBF in this sample. The average organ doses were calculated from the organ doses for each subject independently. To demonstrate the range of individual doses, the minimum and maximum absorbed dose values are given for each organ.

The variability between subjects in the organ dose estimates was expressed as the percent standard deviation (PSD). The PSD was defined as the ratio of the standard deviation to the mean organ dose. This value ranged from a minimum of 5% to a maximum of 66%. Eleven organs had a PSD that was less than 25%: the adrenals, brain, breasts, liver, muscles, pancreas, skin, spleen, testes, thymus and uterus. Five organs had a PSD that was greater than 50%: the gallbladder, small intestine, upper and lower large intestines and the ovaries. The other organs had a PSD between 25% and 50%. The PSD associated with the effective dose equivalent was 35%.

Dosimetry was recalculated based on a theoretical radiolabeling process that used ^{124}I instead of ^{123}I (data available on request). If the contamination with ^{124}I conformed to the manufacturer's specifications, its contribution to the dosimetry was negligible. If the concentration of ^{124}I in our source of radioiodine was 2000 times higher than the manufacturer's guarantee (0.2% instead of 0.0001%), then this positron emitter would have added less than 10% to the absorbed dose to the lower large intestine, and less than 5% to all the other tissues in the model.

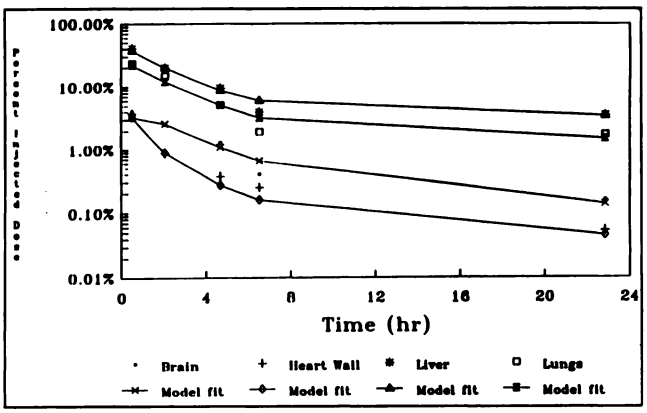

FIGURE 2. Time-activity curves measured in Subject 1.

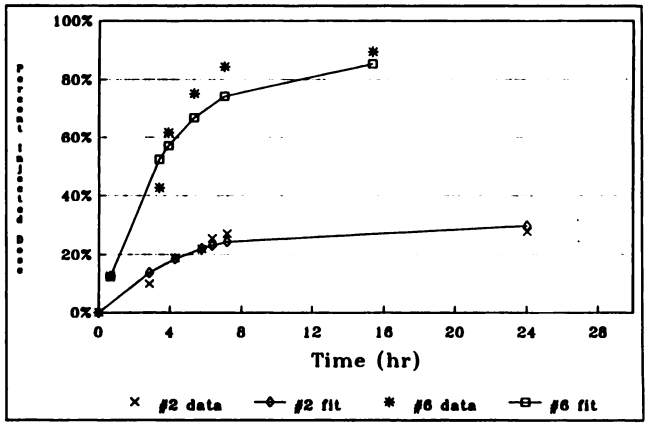

FIGURE 3. Cumulative urinary excretion (measured versus predicted) for two subjects over the first 24 hr postadministration of the ^{123}I-IBF. Subject 1 had the lowest measured urinary excretion fraction, whereas Subject 6 had the largest measured urinary excretion fraction.

DISCUSSION

IBF appears to be a pharmacologically safe radioligand. It did not produce any subjective or objective pharmacological effects in the human volunteers. The lack of an effect is consistent with a substantial body of medical experience which suggests that pharmacological doses of dopaminergic drugs in this range do not have a perceptible effect on humans (*6*).

The radiation exposure associated with IBF appears acceptable for use in human research. The estimates of its dosimetry in this report are probably conservative because problems with the methodology were consistently handled in a way that would increase the calculated exposure. Several features of the protocol used to acquire the images may have resulted in an overestimation of the activity retained in most organs. The relatively large energy window of 20% centered on 159 keV could have permitted internally scattered radiation to contribute to the count rates and increase the apparent activity retention. The high sensitivity collimator may have allowed some downscatter from the high energy photons, which make up about 1.3% of the emissions from ^{123}I. However, the effects of these problems were probably marginal. The errors tended to be canceled out of the calculations by simultaneously imaging the injection syringes containing the doses and the transmission scans with the same camera, collimator and acquisition parameters used to acquire the emission images.

Another systematic error was introduced by multiplying the mean activity per pixel in the center of an organ on the

TABLE 4
Radiation Absorbed Dose Estimates for Iodine-123-IBF

Target organ	Mean (mGy/MBq)	Mean (rad/mCi)	Minimum (mGy/MBq)	Maximum (mGy/MBq)
Adrenals	9.2E-03	3.4E-02	7.7E-03	1.0E-02
Bone surfaces	6.5E-03	2.4E-02	4.4E-03	8.8E-03
Bowel, small‡	4.8E-02	1.8E-01	1.9E-02	9.1E-02
Brain*	4.9E-03	1.8E-02	3.6E-03	6.5E-03
Breasts	2.0E-03	7.4E-03	1.6E-03	2.5E-03
Colon, distal‡	1.3E-01	4.8E-01	5.0E-02	2.6E-01
Colon, proximal‡	1.2E-01	4.4E-01	4.2E-02	2.3E-01
Gallbladder wall‡	7.3E-02	2.7E-01	3.1E-02	1.4E-01
Heart wall*	1.6E-02	5.9E-02	9.9E-03	2.5E-02
Kidneys†	8.3E-02	3.1E-01	4.0E-02	1.3E-01
Liver*	3.5E-02	1.3E-01	2.7E-02	4.2E-02
Lungs*	2.3E-02	8.5E-02	1.6E-02	3.2E-02
Muscle	5.1E-03	1.9E-02	3.7E-03	6.8E-03
Ovaries	2.7E-02	1.0E-01	1.4E-02	4.8E-02
Pancreas	8.7E-03	3.2E-02	6.5E-03	1.1E-02
Red marrow	6.0E-03	2.2E-02	3.7E-03	8.9E-03
Skin	1.7E-03	6.3E-03	1.3E-03	2.2E-03
Spleen	6.2E-03	2.3E-02	4.5E-03	7.4E-03
Stomach‡	7.6E-03	2.8E-02	4.3E-03	1.2E-02
Testes	3.8E-03	1.4E-02	3.5E-03	4.1E-03
Thymus	2.4E-03	8.9E-03	1.9E-03	3.2E-03
Thyroid*	1.1E-02	4.1E-02	4.6E-03	1.5E-02
Urinary bladder†	1.1E-01	4.1E-01	5.8E-02	1.5E-01
Uterus	2.0E-02	7.4E-02	1.6E-02	2.6E-02
Effective Dose Equivalent	[mSv/MBq] 4.3E-02	[rem/mCi] 1.6E-01	[mSv/MBq] 2.7E-02	[mSv/MBq] 6.4E-02

*Calculated from direct measurement of counts in ROI drawn on the images.
†Calculated from direct measurement of counts excreted in the urine.
‡Calculated from direct measurement of counts in a single abdominal ROI.

delayed images by the total number of pixels in the ROI around the earliest image of it. This technique inflated the measurement of the total counts because these small ROIs were placed in the center of each organ, over its region of maximum intensity. The mean activity per pixel in this central ROI was multiplied by the total number of pixels in the ROI of the whole organ on its earliest image, even though the peripheral aspect of most organs was thin and contained significantly less activity than the thicker central region. This effect decreased as the relative size of the ROI increased. But, because the edges of most organs became progressively more obscure as time passed due to the elimination of the tracer, the size of the ROI tended to become smaller and smaller on the delayed images. Part of the error that resulted from using this image analysis technique was reported in an analogous study performed concurrently with another ^{123}I-labeled neuroligand (*43*). Using a limited boundary instead of a whole organ boundary caused the count rates to be overestimated by an average of 4.7%.

Placing small ROIs on the transmission scans also increased the estimates of dosimetry because the method overestimated the effective linear attenuation for each organ. This occurred because the effective linear attenuation for a whole organ was determined from a single measurement in an ROI that was placed over the center of the organs where they tended to be the thickest and attenuate the most photons.

The compartmental model used to calculate the residence times in this study was not a pharmacokinetic model. Rather, it was a mathematical construct that was only useful for fitting the biological data. It had the additional quality of conserving activity in the modeled system. The residence times that were calculated for most of the compartments in the model were relatively insensitive to changes in the L values from the other compartments. This was especially true for the compartments that were not involved in the excretion of the tracer. However, the excretory organ residence times were fairly sensitive to changes in transfer rates from the central compartment. A 10%–20% change in the transfer rate coefficient from the central compartment to the kidneys could have had a noticeable impact on the urinary and fecal excretion distribution fractions, and thus on the urinary bladder and GI residence times. A change of this magnitude (10%–20%) would have resulted in residence time differences of about the same magnitude.

The intersubject variability in transfer rate coefficients was most likely due to two factors. To a smaller extent, the differences probably reflect biological variability and differences in intersubject activity retention. However, the

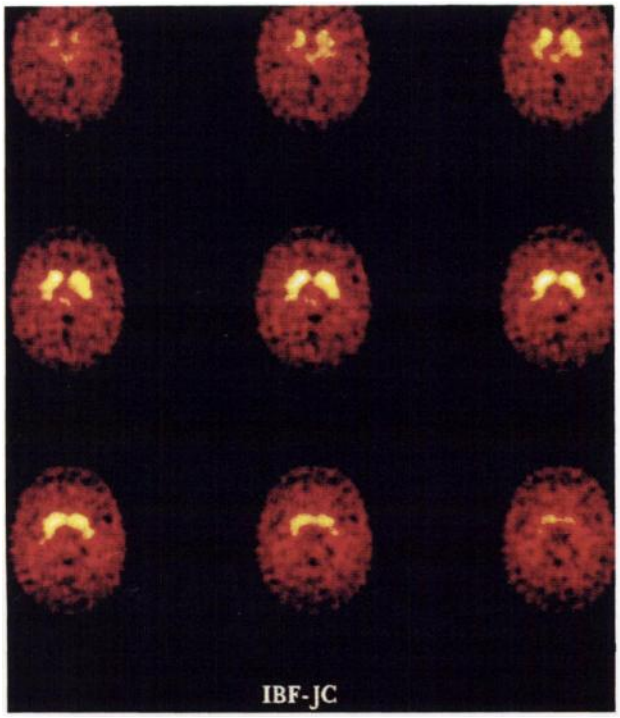

FIGURE 4. Transaxial image of a healthy human brain at the level of the diencephalon. The images were acquired for up to 2 hr after the administration of 5.6 mCi of ^{123}I-IBF on a triple-headed SPECT system (Picker, Cleveland, OH) equipped with fan beam collimators. A count rate dependent prefilter was applied before the images were corrected for attenuation.

factor that probably accounted for most of the differences was that the particular solution surface and local minima could be very different, yet still not significantly affect the residence times or the "goodness" of fit to the data.

Despite these conservative assumptions, the findings suggest that IBF can be used safely in clinical investigations of the D2 dopamine receptor. The amount of activity that can be given will be limited by the dose to the colon. The radiation absorbed doses are low enough to allow more than 370 MBq (10 mCi) of activity to be administered to a healthy volunteer during each study and still fall within federal guidelines for research subjects. Because only about 5 mCi are needed to produce good images of the human brain (Fig. 4), IBF appears to have a large margin of radiation safety in humans.

The true margin of safety in the target organs may be even higher. In clinical practice, the absorbed dose to the urinary bladder wall can probably be reduced substantially by encouraging the subjects to micturate right after the neuroimaging procedure instead of waiting for them to void spontaneously. The absorbed dose to the colon could be decreased by administering a cathartic after the study.

ACKNOWLEDGMENTS

The authors thank Nihon Medi-Physics for providing the necessary funding to conduct the toxicology studies. This study was partially supported by NIH Grant NS-24538 and NIMH grant MH-43880. The work at Oak Ridge was performed under Interagency Agreement No. FDA 224-75-3016, DOE 40-286-71. Oak Ridge Associated Universities performs complementary work for the U.S. Department of Energy under contract DE-AC05-76OR00033.

REFERENCES

1. Alexander GE, Crutcher MD, DeLong MR. Basal ganglia-thalamocortical circuits: parallel substrates for motor, oculomotor, "prefrontal" and "limbic" function. In: Uylings HBM, Van Edin CG, De Bruin JPC, Corner MA, Feenstra MGP, eds. *Progress in brain research, volume 85*. New York: Elsevier Science Publishers; 1990:119–146.
2. Andreasen N, Carson R, Diksic M, et al. Schizophrenia, positron tomography, and dopamine D2 receptors in the human neostriatum. *Schizophr Bull* 1988;14:471–484.
3. Seeman P. Brain dopamine receptors. *Pharmacol Rev* 1980;32:229–269.
4. Stoof J, Kebabian J. Two dopamine receptors: biochemistry, physiology and pharmacology. *Life Sci* 1984;35:2281–2296.
5. Carlsson A. The current status of the dopamine hypothesis in schizophrenia. *Neuropsychopharmacol* 1988;1:179–186.
6. Peroutka SJ, Snyder SH. Relationships of neuroleptic drug effects at brain dopamine, serotonin, α-adrenergic, and histamine receptors to clinical potency. *Am J Psychiatry* 1980;137:1518–1522.
7. Waddington J. Sight and insight: brain dopamine receptor occupancy by neuroleptics visualized in living schizophrenic patients by positron emission tomography. *Br J Psychiat* 1989;154:433–436.
8. Baron JC, Martinot JL, Cambon H, et al. Striatal dopamine receptor occupancy during and following withdrawal from neuroleptic treatment: correlative evaluation by positron emission tomography and plasma prolactin levels. *Psychopharmacol* 1989;99:463–472.
9. Goeders NE, Kuhar MJ. Chronic cocaine administration induced opposite changes in dopamine receptors in the striatum and nucleus accumbens. *Science* 1983;221:773–775.
10. Baxter LR, Schwartz JM, Phelps M, et al. Localization of neurochemical effects of cocaine and other stimulants in the human brain. *J Clin Psychiatry* 1988;49:23–26.
11. Dewey SL, Logan J, Wolf AP, et al. Amphetamine induced decreases in (^{18}F)-N-methylspiroperidol binding in the baboon brain using positron emission tomography (PET). *Synapse* 1991;7:324–327.
12. Volkow ND, Fowler JS, Wolf AP, et al. Distribution and kinetics of carbon-11-cocaine in the human body measured with PET. *J Nucl Med* 1992;33: 521–525.
13. Hall H, Sallemark M, Jerning E. Effects of remoxipride and some related new substituted salicylamides on rat brain receptors. *Acta Pharmacol Toxicol* 1986;340:6–12.
14. Kessler RM, Ansari S, de Paulis T, et al. High affinity dopamine D2 receptor radioligands. 1. Regional rat brain distribution of iodinated benzamides. *J Nucl Med* 1991;32:1593–1600.
15. Hall H, Kohler C, Gawell L. Some in vitro receptor binding properties of [3H] eticlopride, a novel substituted benzamide, selective for the dopamine D2 receptors in the rat brain. *Eur J Pharm* 1985;111:191–199.
16. Janowsky A, de Paulis T, Clanton JA, Smith HE, Ebert MH, Kessler RM. Iodium-125-iodopride: a specific high affinity radioligand for labeling striatal dopamine D2 receptors. *Eur J Pharm* 1988;150:203–205.
17. Kessler R, Ansari M, Schmidt D, et al. High affinity dopamine D2 receptor radioligands. 2. [^{125}I]Epidepride, a potent and specific radioligand for the characterization of striatal and extrastriatal dopamine D2 receptors. *Life Sci* 1991;49:617–628.
18. Kung HF, Pan S, Kung M-P, et al. In vitro and in vivo evaluation of [^{123}I]IBZM: a potential CNS D-2 dopamine receptor imaging agent. *J Nucl Med* 1989;30:88–92.
19. Kung M-P, Liu B-L, Yang Y-Y, Billings JJ, Kung HF. A kit formulation for preparation of ^{123}I-IBZM: a new CNS D-2 dopamine receptor imaging agent. *J Nucl Med* 1991;32:339–342.
20. Kung HF, Alavi A, Chang W, et al. In vivo SPECT imaging of CNS D-2 dopamine receptors: initial studies with ^{123}I-IBZM in humans. *J Nucl Med* 1990;31:573–579.
21. Brucke T, Podreka I, Angelberger P, et al. Dopamine D_2 receptor imaging with SPECT: studies in different neuropsychiatric disorders. *J Cereb Blood Flow Metab* 1991;11:220–228.
22. Schwarz J, Tatsch K, Vogl T, et al. Marked reduction of striatal dopamine D2 receptors as detected by ^{123}IBZM-SPECT in a Wilson's disease patient with generalized dystonia. *Mov Disord* 1992;7:58–61.
23. Seibyl J, Woods S, Zoghbi S, et al. Dynamic SPECT imaging of dopamine

D2 receptors in human subjects with iodine-123-IBZM. *J Nucl Med* 1992; 33:1964–1971.
24. Tatsch K, Schwartz J, Oertel WH, Kirsch CM. SPECT imaging of dopamine D2 receptors with ^{123}I-IBZM in Parkinsonian syndromes. *J Nucl Med* 1991;32:1014–1015.
25. Tatsch K, Schwartz J, Oertel WH, Kirsch CM. SPECT imaging of dopamine D2 receptors with ^{123}I-IBZM: initial experience in controls and patients with Parkinson's syndrome and Wilson's disease. *Nucl Med Commun* 1991; 12:699–707.
26. Verhoeff NP, Brucke T, Podreka I, Bobeldijk M, Angelberger P, Van REA. Dynamic SPECT in two healthy volunteers to determine the optimal time for in vivo D2 dopamine receptor imaging with ^{123}I-IBZM using the rotating gamma camera. *Nucl Med Commun* 1991;12:687–697.
27. Verhoeff NP, Bobeldijk M, Feenstra MG, et al. In vitro and in vivo D2-dopamine receptor binding with [^{123}I]S(−)iodobenzamide ([^{123}I]IBZM) in rat and human brain. *Int J Rad Appl Instrum* 1991;18:837–846.
28. Costa DC, Verhoeff NP, Cullum ID, et al. In vivo characterisation of 3-iodo-6-methoxybenzamide ^{123}I in humans. *Eur J Nucl Med* 1990;16:813–816.
29. Konig P, Benzer MK, Fritzsche H. SPECT technique for visualization of cerebral dopamine D2 receptors. *Am J Psychiatry* 1991;148:1607–1608.
30. Murphy RA, Kung HF, Kung M-P, Billings JJ. Synthesis and characterization of iodobenzamide analogs: potential D-2 dopamine receptor imaging agents. *J Med Chem* 1990;3:171–178.
31. Kung M-P, Kung HF, Billings JJ, Yang Y, Murphy RA, Alavi A. The characterization of IBF as a new selective dopamine D-2 receptor imaging agent. *J Nucl Med* 1990;31:648–654.
32. Robertson J. *Compartmental distribution of radiotracers*. New York: CRC Press; 1983:73–142.
33. Stabin M, Taylor A Jr, Eshima D, Wooter W. Radiation dosimetry for technetium-99m-MAG3, technetium-99m-DTPA and iodine-131-OIH based on human biodistribution studies. *J Nucl Med* 1992;33:33–40.
34. Cloutier RJ, Smith SA, Watson EE, Snyder WS, Warner GG. Dose to the fetus from radionuclides in the bladder. *Health Phys* 1973;25:147–161.
35. Molino G, Hofmann A, Cravetto C. Simulation of the metabolism and enterohepatic circulation of endogenous chenodeoxycholic acid in man using a pharmacokinetic model. *Eur J Clin Invest* 1986;16:397–414.
36. Lawson M, Everson G, Klingensmith W, Kern F Jr. Coordination of gastric and gallbladder emptying after ingestion of a regular meal. *Gastroenterology* 1983;85:866–870.
37. Bobba V, Krishnamurthy G, Kingston E, et al. Gallbladder dynamics induced by a fatty meal in normal subjects and patients with gallstones: concise communication. *J Nucl Med* 1984;25:21–24.
38. International Commission on Radiation Protection. Limits for intake of radionuclides by workers. *ICRP publication 30*. New York: Pergamon Press; 1979:30–34.
39. ICRP Task group report on reference man. *ICRP publication 23*. Oxford: Pergamon; 1975:130–137.
40. Loevinger R, Berman M. A revised schema for calculating the absorbed dose from biologically distributed radionuclides. *MIRD pamphlet no. 1, revised*. New York: Society of Nuclear Medicine; 1975:3–10.
41. Cristy M, Eckerman K. Specific absorbed fractions of energy at various ages from internal photon sources. ORNL/TM-8381/VII. Oak Ridge, TN: Oak Ridge National Laboratory; 1987:7–29.
42. Mozley PD, Zhu XW, Kung HF, et al. The dosimetry of 3-Iodo-Schering 23390: quantification of the radiation burden to healthy humans. *J Nucl Med* 1993;34:208–213.